



ORIGINAL ARTICLE

The NADPH oxidase NOX4 regulates redox and metabolic homeostasis preventing HCC progression

Irene Peñuelas-Haro^{1,2} | Rut Espinosa-Sotelo^{1,2} | Eva Crosas-Molist¹ |
 Macarena Herranz-Iturbide^{1,2} | Daniel Caballero-Díaz^{1,2} | Ania Alay^{3,4} |
 Xavier Solé^{3,4} | Emilio Ramos^{2,5,6} | Teresa Serrano^{2,6,7} |
 María L. Martínez-Chantar^{2,8}  | Ulla G. Knaus⁹ | José M. Cuezva^{10,11} |
 Antonio Zorzano^{12,13,14} | Esther Bertran^{1,2} | Isabel Fabregat^{1,2,15} 

¹TGF- β and Cancer Group, Oncobell Program, Bellvitge Biomedical Research Institute, L'Hospitalet de Llobregat, Barcelona, Spain

²CIBEREHD, ISCIII, Madrid, Spain

³Unit of Bioinformatics for Precision Oncology, Catalan Institute of Oncology, L'Hospitalet de Llobregat, Barcelona, Spain

⁴Preclinical and Experimental Research in Thoracic Tumors, Oncobell Program, IDIBELL, L'Hospitalet de Llobregat, Barcelona, Spain

⁵Department of Surgery, Liver Transplant Unit, University Hospital of Bellvitge, Barcelona, Spain

⁶Faculty of Medicine and Health Sciences, University of Barcelona, L'Hospitalet de Llobregat, Barcelona, Spain

⁷Pathological Anatomy Service, University Hospital of Bellvitge, Barcelona, Spain

⁸Liver Disease Lab, Center for Cooperative Research in Biosciences, Basque Research and Technology Alliance, Bizkaia Technology Park, Spain

⁹Conway Institute, University College Dublin, Dublin, Ireland

¹⁰Center for Molecular Biology "Severo Ochoa," Autonomía University of Madrid, Madrid, Spain

¹¹CIBERER, ISCIII, Madrid, Spain

¹²Biochemistry and Molecular Biomedicine Department, University of Barcelona, Barcelona, Spain

¹³Institute of Research in Biomedicine, Barcelona Institute of Science and Technology (BIST), Barcelona, Spain

¹⁴CIBERDEM, ISCIII, Madrid, Spain

¹⁵Physiological Sciences Department, University of Barcelona, Barcelona, Spain

Correspondence

Isabel Fabregat, Bellvitge Biomedical Research Institute, Avinguda de la Granvia de L'Hospitalet, 199. 08908 L'Hospitalet de Llobregat, Barcelona, Spain.

Email: ifabregat@idibell.cat

Present address

Xavier Solé, Molecular Biology CORE, Center for Biomedical Diagnostics,

Abstract

Background and Aims: The NADPH oxidase NOX4 plays a tumor-suppressor function in HCC. Silencing NOX4 confers higher proliferative and migratory capacity to HCC cells and increases their *in vivo* tumorigenic potential in xenografts in mice. NOX4 gene deletions are frequent in HCC, correlating with higher tumor grade and worse recurrence-free and overall

Abbreviations: DEN, diethylnitrosamine; ECAR, extracellular acidification rate; FA, fatty acid; FAO, fatty acid oxidation; HMOX1, heme oxygenase 1; HUB, Bellvitge University Hospital; MFN1, mitofusin-1; NOX, NADPH oxidase; Nrf2, nuclear factor erythroid 2-related factor 2; NT, nontumor; OCR, oxygen consumption rate; OXPHOS, oxidative phosphorylation; PPAR, peroxisome proliferator-activated receptor; ROS, reactive oxygen species; siRNA, small interfering RNA; T, tumor; WT, wild type.

Esther Bertran and Isabel Fabregat are co-senior authors.

This is an open access article under the terms of the [Creative Commons Attribution-NonCommercial-NoDerivs](https://creativecommons.org/licenses/by-nc-nd/4.0/) License, which permits use and distribution in any medium, provided the original work is properly cited, the use is non-commercial and no modifications or adaptations are made.

© 2022 The Authors. *Hepatology* published by Wiley Periodicals LLC on behalf of American Association for the Study of Liver Diseases.

Hospital Clínic of Barcelona, Translational Genomics and Targeted Therapies in Solid Tumors, August Pi i Sunyer Biomedical Research Institute, Barcelona, Spain

Funding information

Agència de Gestió d'Ajuts Universitaris i de Recerca, Grant/Award Number: 2017SGR1015; Centro de Investigación Biomédica en Red de Enfermedades Hepáticas y Digestivas, Grant/Award Number: CB17/04/00017 and CB06/04/0017; Centro de Investigación Biomédica en Red de Enfermedades Raras, Grant/Award Number: CB06/07/0017; Centro de Investigación Biomédica en Red Diabetes y Enfermedades Metabólicas Asociadas, Grant/Award Number: CB07/08/0017; Ministerio de Ciencia e Innovación, Spain: FPI fellowships : BES-2016-077564, PRE2019-089144, Grant/Award Number: PID2019-106209RB-I00, PID2019-108674RB-I00, SAF2015-64149-R, RTI2018-094079-B-I00, PID2021-122551OB-I00 and RED2018-102576-T; Science Foundation Ireland, Grant/Award Number: 16/IA/4501

survival rates. However, despite the accumulating evidence of a protective regulatory role in HCC, the cellular processes governed by NOX4 are not yet understood. Accordingly, the aim of this work was to better understand the molecular mechanisms regulated by NOX4 in HCC in order to explain its tumor-suppressor action.

Approach and Results: Experimental models: cell-based loss or gain of NOX4 function experiments, *in vivo* hepatocarcinogenesis induced by diethylnitrosamine in *Nox4*-deficient mice, and analyses in human HCC samples. Methods include cellular and molecular biology analyses, proteomics, transcriptomics, and metabolomics, as well as histological and immunohistochemical analyses in tissues. Results identified MYC as being negatively regulated by NOX4. MYC mediated mitochondrial dynamics and a transcriptional program leading to increased oxidative metabolism, enhanced use of both glucose and fatty acids, and an overall higher energetic capacity and ATP level. NOX4 deletion induced a redox imbalance that augmented nuclear factor erythroid 2-related factor 2 (Nrf2) activity and was responsible for MYC up-regulation.

Conclusions: Loss of NOX4 in HCC tumor cells induces metabolic reprogramming in a Nrf2/MYC-dependent manner to promote HCC progression.

INTRODUCTION

The onset and progression of HCC is a multistep process that involves gene mutations in hepatocytes that are subjected to continuous inflammatory and regenerative stimuli.^[1] During malignant transformation and hepatic carcinogenesis, reactive oxygen species (ROS) create an oxidative microenvironment that may generate different types of cellular stress or redox imbalance.^[2] The NADPH oxidase (NOX) family has emerged in the last years as an important source of ROS in signal transduction.^[3,4] Members of the NOX family, such as NOX1, NOX2 and NOX4, produce ROS in the liver, but their role in HCC development and progression is not completely understood yet.^[5] Although NOX1 and NOX2 appear to behave as inducers/promoters of HCC, recent findings postulated NOX4 as a negative regulator of hepatocarcinogenesis. NOX1 and NOX4 showed an opposite pattern in HCC prognosis after hepatectomy (i.e., high NOX1 or low NOX4 expression in patients was associated with worse recurrence-free and overall survival rates).^[6] Higher *NOX4* mRNA expression levels in patients with HCC were significantly associated with prolonged overall survival, whereas increased *NOX1/NOX2* expression significantly correlated with a poor overall survival.^[7] These data suggest that while NOX1 and NOX2 may function as tumor promoters, NOX4 may act as a tumor suppressor in HCC. Supporting this, (i) NOX4 gene deletions are frequent in patients with

HCC, correlating with higher tumor grade,^[8] and (ii) stable knock-down of NOX4 expression in liver cancer cells increased proliferation, migration and invasion, favoring an epithelial-amoeboid transition,^[8,9] and enhanced their tumorigenic potential in mouse xenografts.^[9] Furthermore, *Nox4* expression is down-regulated during liver regeneration after partial hepatectomy in mice,^[9] and *Nox4*-deleted mice showed accelerated recovery of the liver-to-body weight ratio and increased survival.^[10] Despite all of this evidence, the molecular mechanisms governed by NOX4 are not yet understood.

Current studies have focused on the importance of cell metabolic reprogramming during malignant transformation and HCC development.^[11] Therefore, it is crucial to deepen our knowledge about the underlying mechanisms for these alterations to allow diagnostic and therapeutic advancements in HCC treatment.^[12] It has been proposed that HCC cells prefer to generate energy through glycolysis, promoting the conversion of pyruvate into lactate.^[12] A study combining transcriptomics and metabolomics in a panel of paired HCC and adjacent nontumor (NT) tissue demonstrated metabolic remodeling toward a 4-fold enhanced glycolytic metabolism in the tumors when compared with NT tissue.^[13] However, a subgroup of patients characterized by the highest serum alpha-fetoprotein concentrations (as a marker of HCC progression and poorer patient survival) harbored diminished concentrations of certain saturated lipids,

consistent with increased oxidative lipid metabolism. In addition, accumulating evidence supports the importance of lipid metabolic reprogramming in various situations of hepatocarcinogenesis.^[14] Additional work is necessary to fully comprehend the range of metabolic alterations responsible for initiating and promoting HCC tumorigenesis and the molecular mechanisms behind them.

Accordingly, this work aimed to better understand the molecular processes regulated by NOX4 in HCC cells to explain its tumor suppressor action. Data suggest that the loss of NOX4 expression, which occurs in a significant percentage of patients with HCC, induces a redox imbalance that triggers nuclear factor erythroid 2-related factor 2 (Nrf2) activation and MYC-related mitochondrial and oxidative metabolic changes, which may contribute to tumor progression.

MATERIALS AND METHODS

Cell culture

PLC/PRF/5 and Hep3B human HCC cells were from the European Collection of Cell Cultures. SNU449 cells were from the American Tissue Culture Collection. Cell culture conditions, NOX4 knock-down or overexpression, and analyses of cell proliferation and migration are found in the [Supporting Information](#).

Animal models

Nox4^{-/-} (B6.129-Nox4tm1Kkr/J) mice, generated in Dr. Krause's Laboratory, were from Jackson Laboratories (together with the corresponding C57BL/6J wild type [WT] mice). Athymic nude mice were purchased from Harlan Laboratories. Details about mice hosting and *in vivo* experiments are found in the [Supporting Information](#).

Human HCC tissues and ethics statement

Samples from NT and tumor (T) tissues were from patients during surgical procedures at the Bellvitge University Hospital (HUB). Samples derived from a cohort of 128 patients with different etiology were from liver explants at transplantation or resection and incorporated in the study, with most of them in histological grade 2–3, and few in grade 1 or 4 (Table S1). Human tissues were collected with the required informed consent in written from each patient and the approval of the Institutional Review Board (Comité Ético de Investigación Clínica-CEIC, University Hospital of

Bellvitge). Patients' written consent form and the study protocol conformed to the ethical guidelines of the 1975 Declaration of Helsinki.

Immunofluorescence, confocal microscopy, and image quantification

Fluorescence microscopy studies were performed as previously described^[9] (details in the [Supporting Information](#)).

Analysis of the cellular redox balance

Details on all of these methods are found in the [Supporting Information](#).

Proteomic approaches

For high-throughput proteomic analysis, protein extracts of samples were first digested with trypsin, and then the peptides were labeled with the iTRAQ isobaric tags. Western blotting was carried out as previously described.^[8] Primary antibodies are summarized in Table S2. Further details are found in the [Supporting Information](#).

Gene-expression analyses

Details on all of these methods are found in the [Supporting Information](#).

Analysis of cell metabolism

Cell samples (100 μ l of cell pellet, five replicates for each group) were submitted for metabolic profiling to Metabolon Inc. ATP quantification was measured using the ATP Bioluminescence Assay Kit CLS II (Sigma-Aldrich), following the manufacturer's instructions. L-lactate concentration was determined using an enzymatic reaction, and glucose concentration was determined using a glucose oxidase and peroxidase method, as previously described.^[15] The Seahorse analyzers XFe96 and XF24 (Agilent) were used to continuously monitor the oxygen consumption rate (OCR) and extracellular acidification rate (ECAR), respectively, as previously described.^[15] The mitochondrial-to-nuclear DNA ratio was assessed by real-time PCR using the Human Mitochondrial DNA Monitoring Primer Set Ratio kit (Takara Bio). Further details on all of these methods can be found in the [Supporting Information](#).

Data analysis

Details are found in the [Supporting Information](#).

RESULTS

Inverse correlation between NOX4 and MYC in HCC

Models of loss and gain of NOX4 function in HCC cells, generated in previous studies,^[8] were used in this work. NOX4 was knocked down by short hairpin RNA (shRNA) technology in the epithelial cell line PLC/PRF/5, which expresses high levels of NOX4. In the more migratory mesenchymal-like invasive cell line SNU449, which expresses low NOX4 levels, the human NOX4 gene was overexpressed (Figure S1A,B). NOX4 silencing or overexpression correlated with a decrease or increase in cellular H₂O₂ production, respectively (Figure S1C). Silencing NOX4 in PLC/PRF/5 cells induced cell proliferation and migration, whereas overexpression of NOX4 in SNU449 cells caused the opposite effects (Figure S1D,E). In these cell lines we performed iTRAQ proteomic analysis, which strongly pointed out the overactivation of the MYC pathway in PLC/PRF/5 cells after silencing NOX4 (Figure 1A) and its inhibition in SNU449 cells after overexpressing NOX4 (Figure S2).

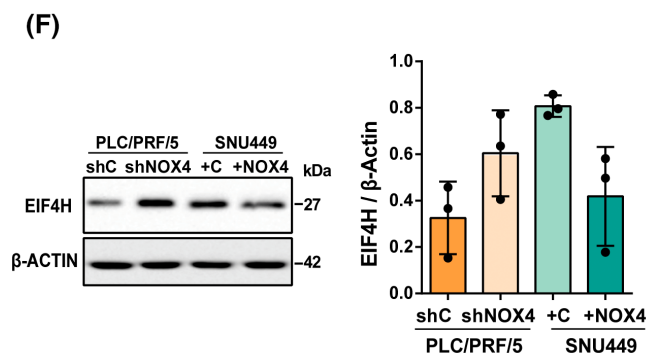
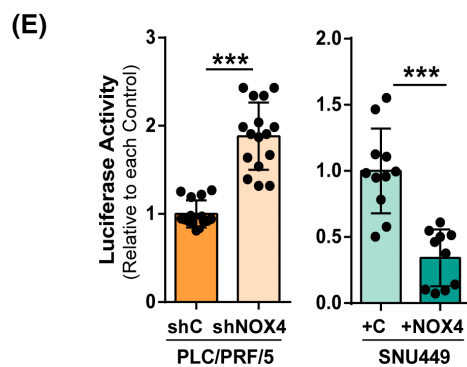
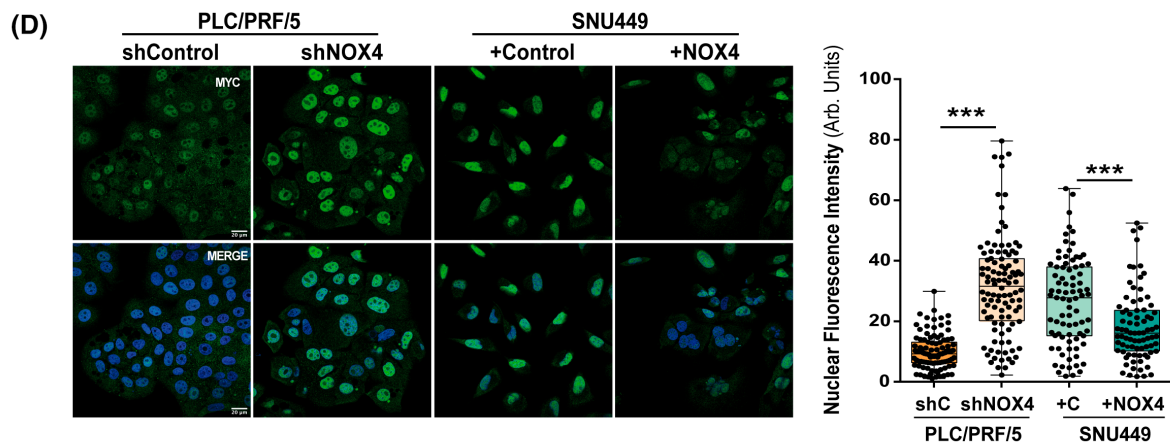
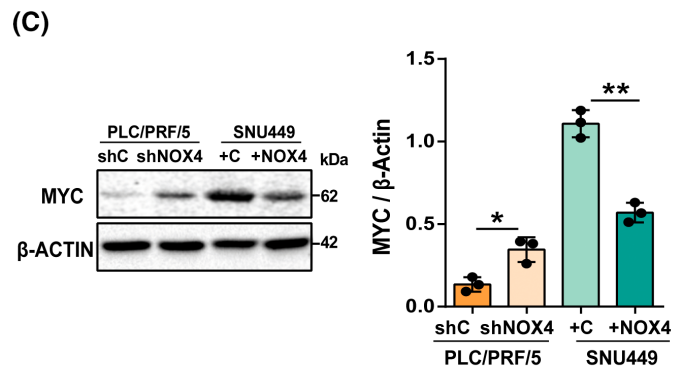
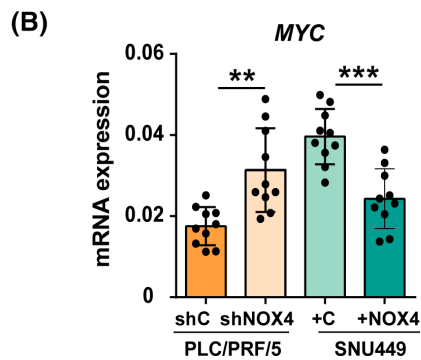
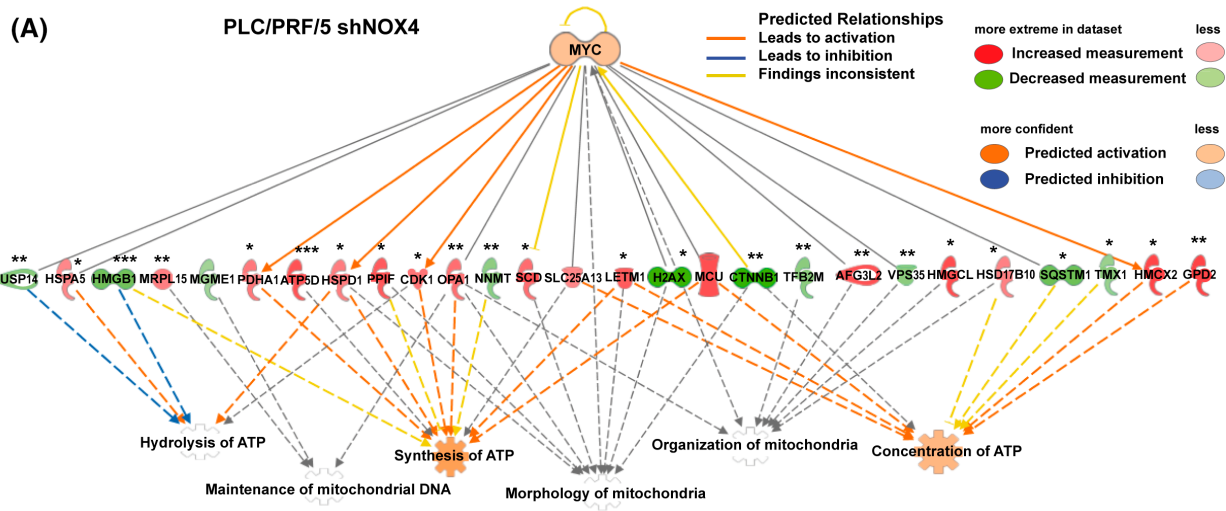
Considering these results, we decided to explore MYC expression and activity further. As shown in Figure 1B,C, silencing NOX4 in PLC/PRF/5 cells significantly increased MYC mRNA and protein levels, whereas overexpression of NOX4 in SNU449 decreased them. Furthermore, immunocytochemical analysis of MYC revealed concomitant differences in its nuclear content, which significantly increased in shNOX4-PLC/PRF/5 cells and decreased in SNU449+NOX4 cells (Figure 1D). Luciferase reporter assays revealed higher MYC transcriptional activity in shNOX4-PLC/PRF/5 cells and lower activity in SNU449+NOX4 cells, which correlated with differences in the levels of one of its targets, EIF4H (Figure 1E,F). To analyze whether NOX4 activity is required for the observed effects, we overexpressed in parallel an active or a mutated inactive form of NOX4 in SNU449 cells (Figure S3A) and ascertained that the NOX4 mutant was not active and

did not generate H₂O₂ (Figure S3B), and CYBA gene expression (regulated by NOX4) was up-regulated by the WT, but not the mutated form (Figure S3A). Effects on cell proliferation and migration were not observed in the NOX4 mutant transfected cells (Figure S3C,D), and MYC intranuclear localization and activity were not altered (Figure S3E,F).

We then wished to determine whether these observations have *in vivo* relevance and promoted hepatocarcinogenesis mediated by diethylnitrosamine (DEN) in WT and *Nox4*^{-/-} mice (Figure S4A). *Nox4* expression in WT mice showed a tendency to decrease in livers at 9 months after treatment, where pre-neoplastic nodes, but not big tumors, can be microscopically observed (Figure S4B). After 11 months, when the T can be separated from the NT tissue, in WT mice *Nox4* expression was decreased in tumor when compared with NT tissue. The WT animals presented clearly small visible tumors (at least one), but most of them lower than 5-mm diameter; only one mouse presented two tumors of higher size, around 8–9 mm each (Figure S4C,D, top images). In *Nox4*^{-/-} mice from the five mice incorporated in the study, two of them showed a necrotic liver and apparent hepatomegaly with numerous small tumors extending through the liver, and the appearance of a spongy liver. In the other three mice, very large tumors were observed in two of the cases with a size of approximately 2 cm (Figure S4C,D, bottom images). Tumors in *Nox4*^{-/-} mice showed higher proliferative capacity as analyzed by Ki67 immunohistochemistry (Figure 2A). Interestingly, analysis of *Myc* mRNA levels revealed significantly higher expression in PBS-treated livers of *Nox4*^{-/-} mice when compared with WT mice (Figure S4E). When *Myc* expression was analyzed in DEN-induced tumors after 11 months of treatment, we observed significant higher expression in the T when compared with NT areas (Figure 2B). High *Myc* expression and increased tumor size were correlated. These observations indicate that deletion of *Nox4* in mice affects certain facets of the hepatocarcinogenesis process and, similar to our cell-based studies, increased cell proliferation, correlating with higher *Myc* expression is observed in *Nox4*^{-/-} tumors.

Next, we explored NOX4 and MYC expression in T versus NT (T/NT) tissues in a cohort of 128 human HCC tumors from patients submitted to surgical intervention in the HUB. We distributed NOX4 and MYC

FIGURE 1 MYC expression and activation inversely correlates with NADPH oxidase (NOX4) levels. (A) Ingenuity Pathway Analysis of proteomic data in PLC/PRF/5 shNOX4 cells compared with shControl cells. Edges and nodes are color-coded based on the predicted relationship as indicated in the prediction legend. (B) Relative MYC mRNA expression. Data are presented as mean ± SD (*n* = 10). (C) Left: MYC protein levels. β-Actin was used as loading control. Right: Densitometric analysis, expressed as relative to β-Actin. Data are presented as mean ± SD (*n* = 3). (D) Left: Immunofluorescence of MYC (green) and DAPI (blue) for nuclei staining. Scale bar, 20 μm. Right: Quantification of nuclear fluorescence intensity. Each dot represents one nucleus. (E) Transcriptional MYC activity. Results are shown relative to each control. Data are presented as mean ± SD (*n* = 12–16). (F) Left: EIF4H protein levels. β-Actin was used as loading control. Right: Densitometric analysis, expressed as relative to β-actin. Data are presented as mean ± SD (*n* = 3). **p* < 0.05, ***p* < 0.01, ****p* < 0.001



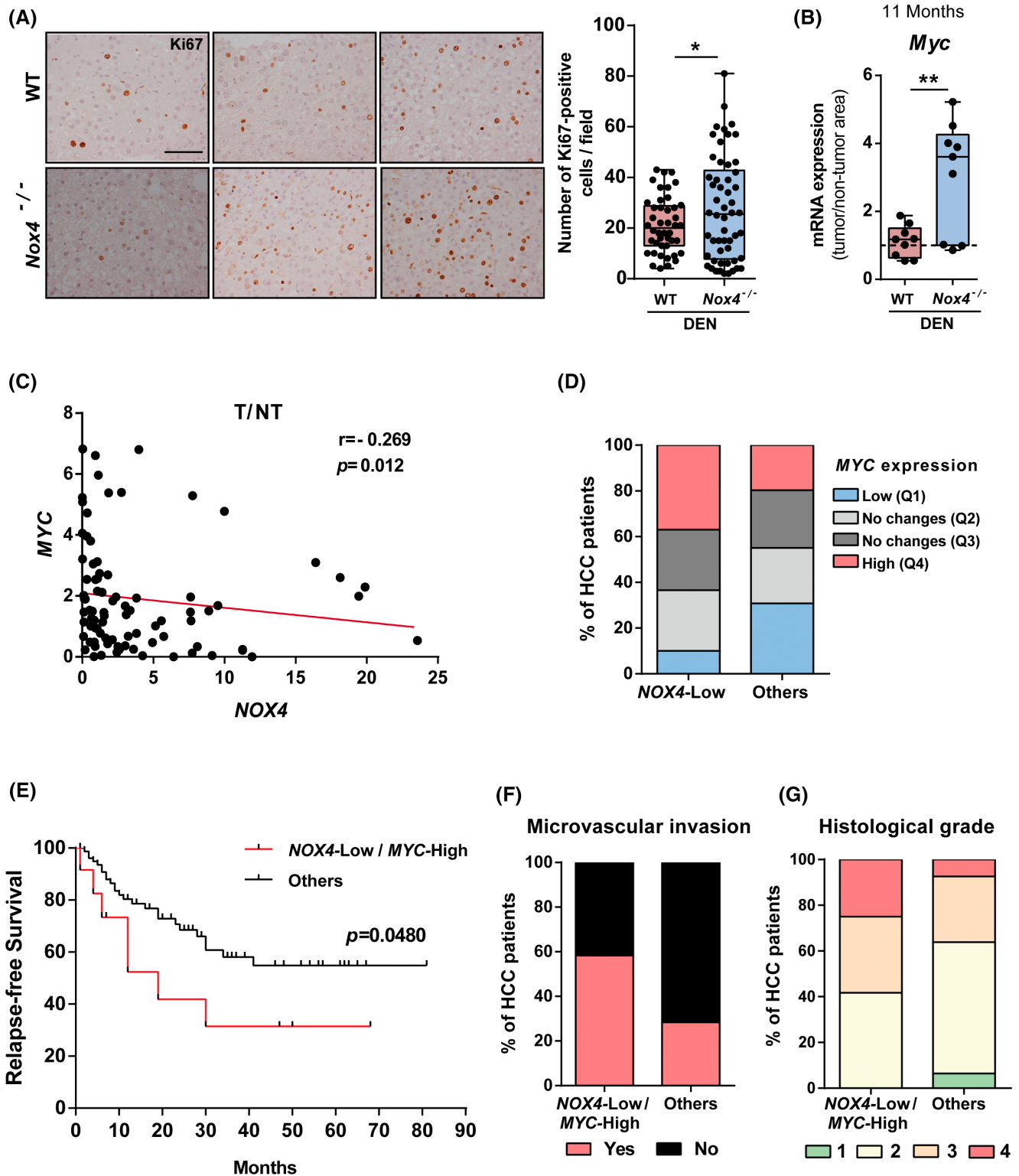


FIGURE 2 Analysis of *Nox4/NOX4* and *Myc/MYC* expression in mice/human under a hepatocarcinogenic process (see Figures S4 and S5 for complementary information). (A) Ki67 immunohistochemistry in tumors from wild-type (WT) and *Nox4*^{-/-} mice at 11 months following diethylnitrosamine (DEN) treatment. Scale bar, 50 μm. Right: Quantification of positive nuclei. Each dot represents one nucleus. (B) *Myc* mRNA expression in tumor (T) and nontumor (NT) areas from WT and *Nox4*^{-/-} mice at 11 months following DEN treatment. Data are presented as a ratio. (A,B) Results are expressed as box plots with whiskers (min to max) ($n = 9$; 3 lysates from 3 different animals). (C) Pearson correlation analysis of the ratio T/NT between *NOX4* and *MYC* gene expression in all patients used in the study. (D) *MYC* expression in *NOX4*-low (Q1) patients versus the others, expressed as a percentage. (E) Kaplan–Meier curve for relapse-free survival in patients with *NOX4*-low/*MYC*-high HCC versus the others. (F,G) Percentage of patients with HCC according to microinvasion (F) and histological grade (G) in patients with *NOX4*-low/*MYC*-high HCC versus other patients. Differences are considered statistically significant when p -values < 0.05 . ** $p < 0.01$

expression from patients in four quartiles for further comparative analysis and correlation (Figure S5A). A great heterogeneity could be found in the expression of *NOX4*, but about 30% of the patients presented a T/NT ratio lower than 1 (Q1 and part of Q2; Figure S5A, left). Regarding etiology, patients with low *NOX4* expression (Q1) presented a higher proportion of hepatitis C virus and higher cirrhotic background (Figure S5B,C). Considering the data from all of the patients, the T/NT expression of *NOX4* and *MYC* negatively correlated ($p = 0.012$) (Figure 2C), and the percentage of patients in Q1 (low) for *NOX4* expression showed a higher number of patients in Q4 (high) for *MYC* expression (Figure 2D). It is important to note that HUB patients with low *NOX4* and high *MYC* expression showed lower relapse-free survival than all of the other patients (Figure 2E). Interestingly, although data must be taken with caution due to the limited number of patients, younger patients (age lower than 65 years) showed much worse relapse-free survival (Figure S5D). Finally, about 60% of patients with low *NOX4* and high *MYC* expression showed microvascular invasion versus about 25% in the other groups (Figure 2F) and had a more advanced histological grade (Figure 2G). In conclusion, these data point to the *NOX4*/*MYC* axis as a component of the complex hepatocarcinogenesis process, which could be relevant in the progression of a significant percentage of patients with HCC.

The axis *NOX4*/*MYC* regulates mitochondrial morphology and oxidative metabolism in HCC

The iTRAQ proteomic analysis in HCC cells with silenced or overexpressed *NOX4* revealed that processes such as morphology, organization, and function of the mitochondria, as well as ATP synthesis, occurred downstream of *MYC* (Figure 1A and Figure S2). In fact, mitochondria morphology significantly changed, increasing in size and with elongated shape, and altered the number of branches and branch length in sh*NOX4* PLC/PRF/5 cells when compared with their controls. In contrast, overexpression of *NOX4* in SNU449 cells induced opposite changes (Figure 3A). Changes in mitochondrial morphology correlated with changes in the intracellular content of ATP, which increased in sh*NOX4* PLC/PRF/5 cells and decreased in *NOX4*-overexpressing SNU449 cells, when compared with their respective controls (Figure 3B). Sh*NOX4* PLC/PRF/5 cells presented an increase in mitochondrial DNA copy number (Figure 3C) and higher levels of proteins related to mitochondrial dynamics, such as the pro-fusion mitofusin-1 (MFN1), mitofusin-2 (MFN2) and OPA1 mitochondrial dynamin-like GTPase, and of the pro-fission dynamin-related GTPase 1, which are

essential for normal mitochondrial morphology by regulating the equilibrium between mitochondrial fusion and fission (Figure 3D).

Connecting with the changes in mitochondrial function and ATP synthesis, a more detailed analysis of the iTRAQ proteomic data also revealed a strong cross-talk between *NOX4* and metabolic pathways (Figure S6A). Oxidative phosphorylation (OXPHOS) was the most significant pathway altered in PLC/PRF/5 cells after targeting *NOX4* for knockdown (Figure S6B). For this reason, we decided to explore the OCR in both cell lines after loss or gain of *NOX4* function. Results clearly demonstrated that in sh*NOX4* PLC/PRF/5 cells, the basal, ATP-linked, maximal, and reserve OCR were significantly increased when compared with shControl cells (Figure 3E, left and middle). On the contrary, OCR was significantly decreased at all levels in *NOX4*-overexpressing SNU449 cells (Figure 3F, left and middle). Using a specific array for the transcriptomic analysis of metabolic/mitochondrial-related genes (Figure 3E,F, right), or detailed examination of the proteins whose levels showed differences in the iTRAQ proteomic analysis (Figure S7), we found increased levels of different mRNAs/proteins related to mitochondrial oxidative metabolism, components of the mitochondrial electronic transport chain, or ATP synthase complex, when knocking down *NOX4* in PLC/PRF/5 cells. Some of these genes clearly presented the opposite trend (i.e., decreased expression) in SNU449 cells after the overexpression of *NOX4*. Western blot analysis of the different components of the respiratory chain confirmed regulation of subunit 2 of cytochrome c oxidase or ATP synthase subunit beta (Figure 3G).

Next, we considered whether the regulation of *MYC* could be responsible for the changes observed in mitochondria and oxidative metabolism after silencing *NOX4*. After transient knockdown of *MYC* by small interfering RNA (siRNA) in sh*NOX4* PLC/PRF/5 cells, which decreased cellular proliferation and migration (Figure 4A), a reversal of the changes in mitochondrial morphology (Figure 4B) and in the levels of mitochondrial dynamics proteins (Figure 4C) was observed. Silencing *MYC* induced a significant decrease in the basal, ATP-linked, or maximal OCR levels in sh*NOX4* PLC/PRF/5 (Figure 4D), which correlated with a decrease in oxidative metabolism-related proteins (Figure 4E) and cellular ATP content (Figure 4F). At the transcriptional level, transient knockdown of *MYC* induced the down-regulation of metabolic/mitochondria-related genes, specifically in sh*NOX4* PLC/PRF/5 cells (Figure 4G). Knockdown of *NOX4* in PLC/PRF/5 also induced an increase in ECAR (Figure S8A), which reflects the glycolytic capacity of the cells, which was attenuated after silencing *MYC* (Figure S8B). Overall, these results indicate that loss of *NOX4* induces remodeling of mitochondrial dynamics and reprogram metabolism in a *MYC*-dependent manner.

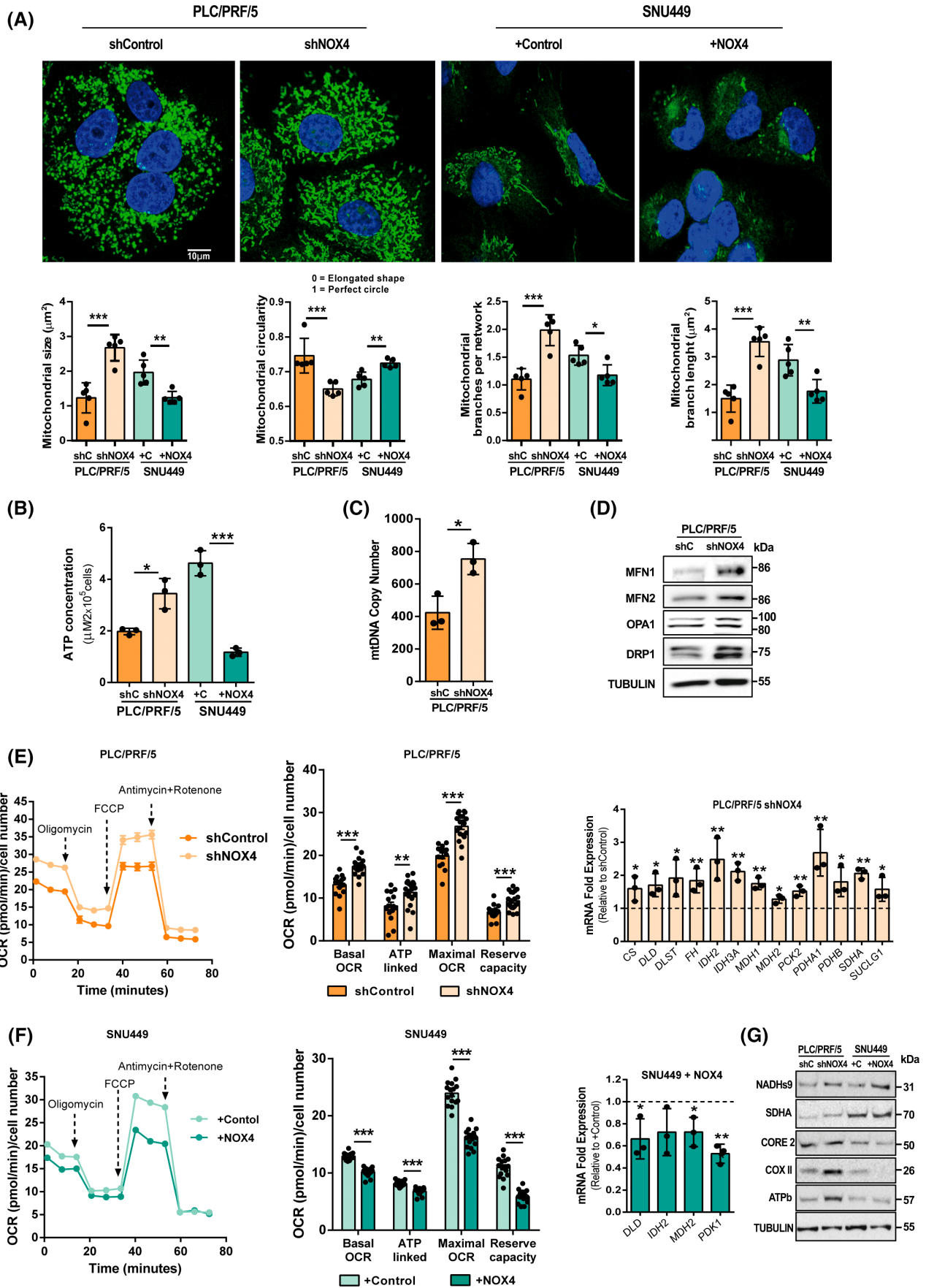


FIGURE 3 Low levels of NOX4 correlate with a more elongated mitochondrial phenotype, higher respiration capacity, and ATP production. (A) Top: Immunocytochemical analysis of mitochondrial ATP synthase subunit beta (ATPb) in green. DAPI (blue) was used for nuclei staining. Scale bar, 10 μ m. Bottom: Quantification of mitochondrial size, circularity, branches per network, and branch length. Each dot represents the average of all mitochondria from independent experiments ($n = 5$). (B) Intracellular ATP levels normalized to cell number. Data are presented as mean \pm SD ($n = 3$). (C) Mitochondrial to nuclear DNA ratio. Data are presented as mean \pm SD ($n = 3$). (D) Mitochondrial dynamics-related protein levels. Tubulin was used as loading control. A representative experiment is shown. (E,F) Seahorse analysis of oxidative phosphorylation (OXPHOS) in PLC/PRF/5 (E) and SNU449 (F) HCC cells. Left: Continuous oxygen consumption rate (OCR) values ([μ moles O_2 /min]/cell number) are shown. Middle: Bar graphs of mitochondrial functions were analyzed as explained in the [Supporting Information](#). Data are presented as the mean \pm SEM ($n = 9-12$). Right: Fold mRNA expression of different genes related to OXPHOS. Top: PLC/PRF/5 shNOX4. Bottom: SNU449 + NOX4, normalized to each control. Data are presented as mean \pm SD ($n = 3$). (G) Electron transport chain-related protein levels. Tubulin was used as loading control. A representative experiment is shown. * $p < 0.05$, ** $p < 0.01$, *** $p < 0.001$. CS, citrate synthase; *DLD*, dihydroliipoamide dehydrogenase; *DLST*, dihydroliipoamide S-succinyltransferase; *FH*, fumarate hydratase; *IDH2*, isocitrate dehydrogenase 2; *IDH3A*, isocitrate dehydrogenase 3A; *MDH1*, malate dehydrogenase 1; *MDH2*, malate dehydrogenase 2; *PCK2*, phosphoenolpyruvate carboxykinase 2; *PDHA1*, pyruvate dehydrogenase E1 subunit alpha 1; *PDHB*, pyruvate dehydrogenase E1 subunit beta; *SDH*, succinate dehydrogenase complex flavoprotein subunit A; *SUCLG1*, succinate-CoA ligase GDP-ADP forming subunit alpha.

NOX4 regulates both glucose and fatty acid metabolism

In light of the relevant effect of silencing or overexpressing NOX4 on metabolism of HCC cells, we decided to perform a complete metabolomic analysis. Results pointed to lipid metabolism as highly affected. In shNOX4 PLC/PRF/5 cells, decrease in diacylglycerols and increase in monoacylglycerols occurred (Table S4 and Figure 5A, left) which could reflect an increase in lipolysis, whereas in the NOX4-overexpressing SNU449 cells, carnitine intermediates accumulated (Table S5 and Figure 5A, right), which could indicate decreased fatty acid oxidation (FAO). The expression of different genes related to lipid catabolism, or to its regulators, such as the peroxisome proliferator-activated receptor (PPAR) family, was significantly increased in shNOX4 PLC/PRF/5 cells and decreased in NOX4-overexpressing SNU449 cells (Figure 5B). The proteomic analysis previously had revealed changes in the FAO pathway in shNOX4 PLC/PRF/5 cells (Figure S6B), and an independent analysis of different proteins related to fatty acid (FA) catabolism uncovered increased levels in shNOX4 PLC/PRF/5 cells and decreased levels in NOX4-overexpressing SNU449 cells (Figure 5C). Transient knockdown of MYC induced the down-regulation of genes related to FA catabolism, specifically in shNOX4 PLC/PRF/5 cells (Figure 5D), which positions MYC activity upstream of the transcriptional changes in genes related to lipid metabolism in NOX4-silenced cells.

To further evaluate changes in the glycolytic capacity of the cells, we performed a more detailed analysis of ECAR. Results revealed that shNOX4 PLC/PRF/5 cells had higher glycolytic capacity and glycolytic reserve (Figure 6A), which correlated with an increase in the expression of certain genes related to the glycolytic pathway (Figure 6B, left). In contrast,

the expression of some glycolysis-related genes appeared to be decreased in NOX4-overexpressing SNU449 cells (Figure 6B, right). The analysis of glucose consumption and glucose-6-phosphate levels (reflecting its use) revealed an increase in shNOX4 PLC/PRF/5 cells and a decrease in NOX4-overexpressing SNU449 cells, when compared with their respective controls (Figure 6C). Analysis of lactate production and lactate dehydrogenase A expression (Figure 6D) further confirmed the effect of NOX4 on the glycolytic pathway and indicated that glucose could be also metabolized toward lactate. These results suggest that NOX4 is controlling cellular metabolism by regulating both glycolysis and mitochondrial oxidative metabolism, with all effects combined contributing to the relevant differences in ATP levels observed in cells in which NOX4 was attenuated or overexpressed (Figure 3B).

To corroborate these results in an additional HCC cell line, we stably knocked down NOX4 with shRNA in the Hep3B cells, which express high levels of NOX4. The changes observed in proliferation, migration, MYC expression, OCR, ECAR, or lipid metabolomics in these cells were identical to those observed in the shNOX4-PLC/PRF/5 cells (Figure S9).

Interestingly, analyzing the Roessler public database of T and NT gene expression in HCC human samples, we found a strong and significant inverse correlation between NOX4 expression and some of the most significant metabolic genes found in *in vitro* experiments, such as acyl-CoA synthetase long chain family member 5, isocitrate dehydrogenase 1, solute carrier family 27 member 2, phosphofructokinase liver type, or the master regulator gene peroxisome proliferator activated receptor alpha. A significant inverse correlation with *MFN2* was also observed (Figure S10).

Overall, these results strongly suggest a role for NOX4 in regulating metabolic homeostasis in HCC.

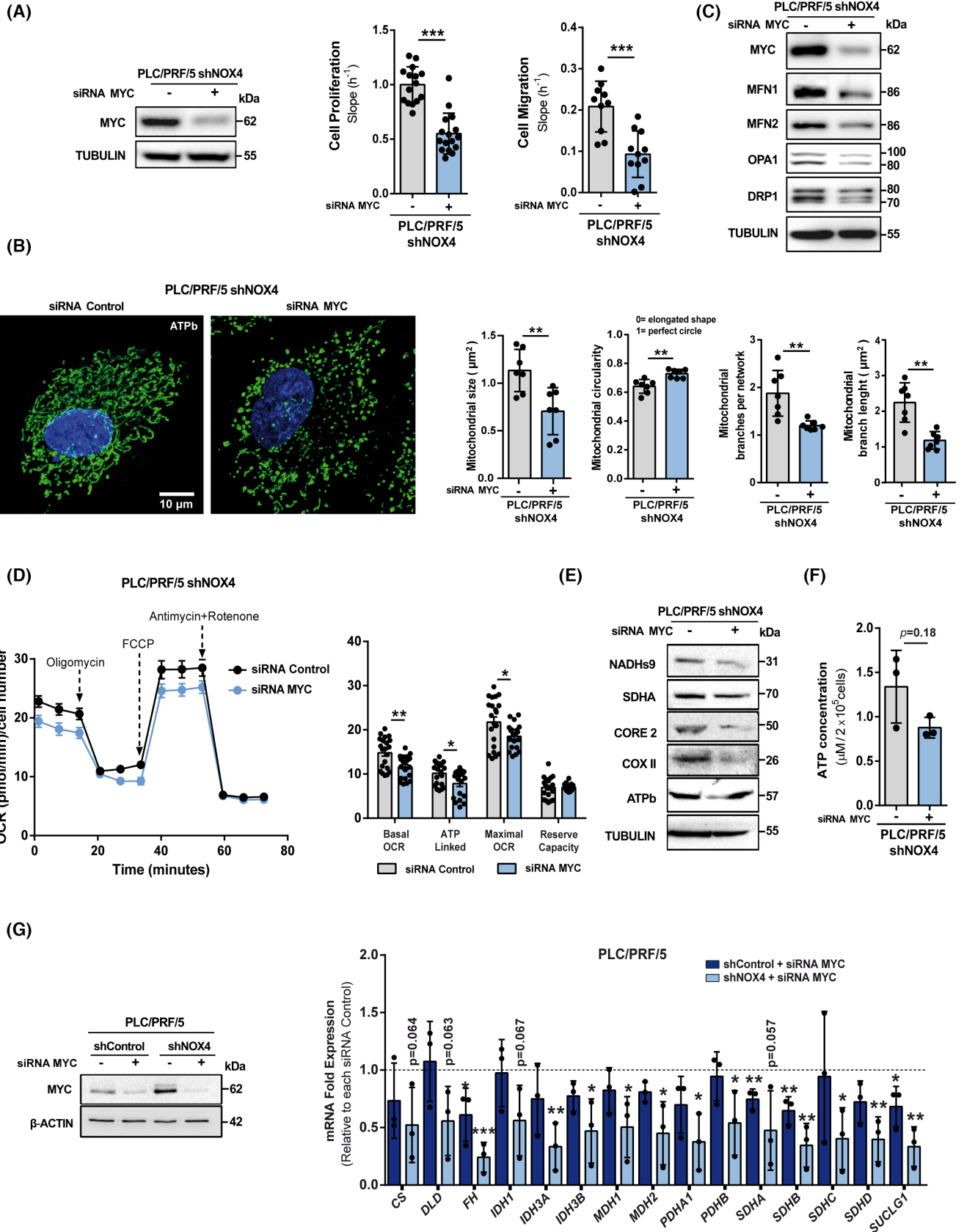


FIGURE 4 MYC mediates the changes observed in mitochondrial phenotype, respiration capacity, and transcriptional reprogramming of OXPHOS-related genes in NOX4 silenced cells. (A–F) PLC/PRF/5 shNOX4 were transiently transfected either with control or MYC-specific small interfering RNA (siRNA) sequences for 48 h. (A) Left: MYC protein levels. β -Actin was used as loading control. A representative experiment is shown. Middle: Cell proliferation at 72 h. Right: Cell migration at 8 h. Results are expressed as slope (h^{-1}). Data are presented as mean \pm SEM ($n = 10$ –16). (B) Left: Immunocytochemistry of ATPb in green and DAPI (blue). Scale bar, 10 μ m. Right: Quantification of mitochondrial size, circularity, branches per network, and branch length. Each dot represents the average of all mitochondria from independent experiments ($n = 7$). (C) Mitochondrial dynamics–related protein levels. Tubulin was used as loading control. A representative experiment is shown. (D) Seahorse analysis of OXPHOS. Left: Continuous OCR values ($[pmoles\ O_2/min]/cell\ number$) are shown. Right: Bar graphs of mitochondrial functions were analyzed as explained in the [Supporting Information](#). Data are presented as mean \pm SEM ($n = 9$ –12). (E) Electron transport chain–related protein levels. Tubulin was used as loading control. A representative experiment is shown. (F) Intracellular ATP levels normalized to cell number. Data are presented as mean \pm SD ($n = 3$). (G) PLC/PRF/5 cells were transiently transfected either with control or MYC-specific siRNA sequences for 48 h. Left: MYC protein levels. β -Actin was used as loading control. A representative experiment is shown. Right: OXPHOS-related gene expression. Results are expressed as fold mRNA expression, in which each MYC siRNA condition was normalized to its respective unspecific sequence. Data are presented as mean \pm SD ($n = 3$). * $p < 0.05$, ** $p < 0.01$, *** $p < 0.001$. FH, fumarate hydratase; SDHB, succinate dehydrogenase complex iron sulphur subunit B; SDHC, succinate dehydrogenase complex subunit C; SDHD, succinate dehydrogenase complex subunit D.

NOX4 loss activates Nrf2, which mediates MYC activation

To deepen the molecular mechanisms that connect NOX4 and MYC, we focused on the iTRAQ proteomic analysis in cell lines in which NOX4 had been silenced or overexpressed. From this analysis, Nrf2 was identified as one of the pathways clearly modulated by NOX4 expression (Figure S11). A significant increase in Nrf2 protein levels (Figure 7A), nuclear localization (Figure 7B), antioxidant response element (ARE) transcriptional activity (Figure 7C), and the expression of two Nrf2 target genes (NADPH dehydrogenase quinone 1-*NQO1* and Heme oxygenase 1-*HMOX1*) were observed in shNOX4 PLC/PRF/5 cells, corroborating the changes of HMOX1 at the protein level (Figure 7D). A decrease in all of these parameters was visualized in NOX4-overexpressing SNU449 cells. The analysis of tumor samples from DEN-treated mice also revealed a significantly higher expression of the Nrf2 target genes *Hmox1* and *Nqo1* in tumors from *Nox4*^{-/-} mice, but not in tumors from WT mice (Figure 7E). Additionally, we explored the expression of MYC and Nrf2 target genes in a model of subcutaneous xenograft tumors by implantation of Hep3B cells (control and NOX4 knock-down cells) (Figure S12A). We previously reported that tumors from shNOX4 Hep3B cells developed earlier and were higher in size.^[9] Using those tumor tissues, we observed a higher expression of MYC and Nrf2 target genes *HMOX1* and *NQO1* (Figure S12B). Overall, an inverse correlation between NOX4 expression and Nrf2 activity was observed in HCC, both *in vitro* and *in vivo*. Next, we decided to analyze the effect of siRNA-mediated transient Nrf2 knockdown on MYC levels in shNOX4 PLC/PRF/5 cells. As observed in Figure 7F, attenuating Nrf2 strongly affects the MYC protein levels, whereas attenuating MYC did not affect Nrf2 protein levels. Similarly, MYC mRNA levels and MYC transcriptional activity were significantly decreased in shNOX4 PLC/PRF/5 cells after knocking down Nrf2 (Figure 7F). These data would indicate that loss of NOX4 activates

the Nrf2 pathway, which directly or indirectly would regulate MYC levels and activity.

A detailed analysis of oxidative stress markers revealed inverse correlation among NOX4 and oxidative protein modifications, such as carbonylations or nitrations (Figure S13A,B). The metabolomic analysis also revealed inverse correlation with amino acid oxidation, as the levels of methionine sulfone or sulfoxide derivatives showed (Figure S13C). Levels of reduced or oxidized glutathione were not significantly changed, but NOX4 expression inversely correlated with ophthalmate levels, a biomarker of oxidative stress, which reflects higher glutathione use and subsequent increase in its synthesis (Figure S13D). All of these results indicate that NOX4 acts as a regulator of the redox homeostasis in HCC, and its loss may produce a situation of higher oxidative stress that justifies the activation of the Nrf2 pathway.

Higher oxidative stress could be related to an increase in mitochondrial ROS. However, we could not find any increase in mitochondrial superoxide content, analyzed with MitoSOX, in shNOX4 PLC/PRF/5 cells (results not shown). Because we had previously found an inverse correlation between the expression of NOX4 and other NOXs, in particular NOX1,^[16–18] we hypothesized that levels of NOX4 could affect the levels of other members of the family (Figure 8A). PLC/PRF/5 cells express substantial levels of NOX1 and NOX2. Attenuation of NOX4 expression in the shNOX4 cells induced a significant increase in NOX1. SNU449 cells only express NOX2, and its expression was reduced after overexpressing NOX4. We could not find differences in nitric oxide synthases gene expression, but nitrite levels, which reflect nitric oxide oxidation, inversely correlated with NOX4 levels (Figure 8B). Knocking down NOX1 in shNOX4 PLC/PRF/5 cells or NOX2 in NOX4-overexpressing SNU449 cells significantly decreased both ARE and MYC transcriptional activity (Figure 8C,D). Furthermore, inhibition of NOXs with diphenyliodonium chloride or use of the general antioxidant GKT136 decreased MYC activation in PLC/

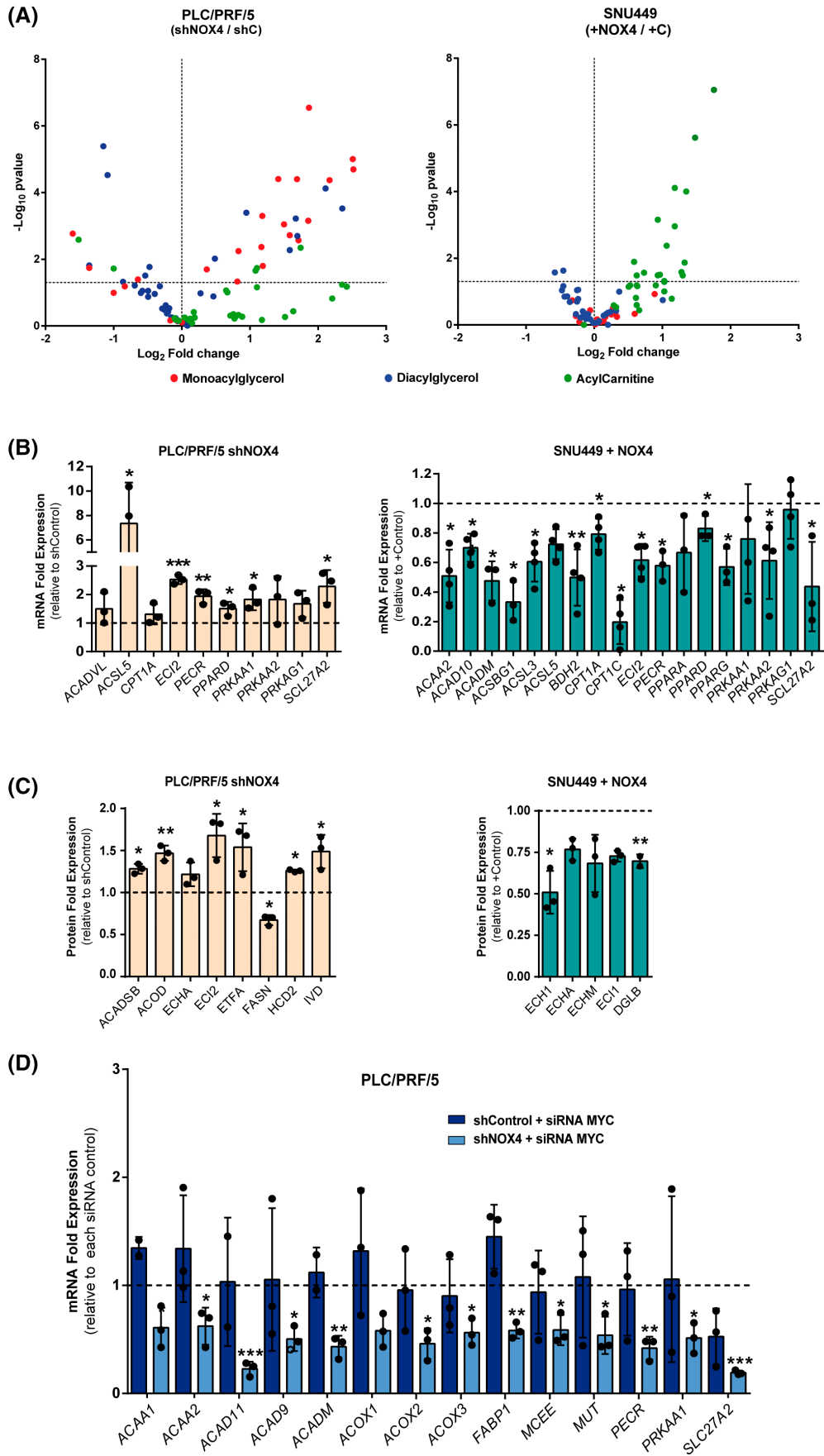


FIGURE 5 The axis low NOX4/high MYC increases lipid catabolism. (A) Volcano plot of metabolites related to metabolism of monoacylglycerol, diacylglycerol, and acylcarnitine intermediates. It is represented as fold change relative to each control ($n = 6$ for each group). Detailed information of depicted metabolites is provided in Tables S4 and S5. (B) mRNA fold expression of lipid metabolism-related genes, relative to each control. Data are presented as mean \pm SD ($n = 3$). (C) Lipid metabolism-related protein levels (from proteomics analysis), shown as ratio to each respective control. Data are presented as mean \pm SD ($n = 3$). (D) PLC/PRF/5 shControl and shNOX4 cells were transiently transfected either with control or MYC-specific siRNA sequences for 48 h. Expression of lipid metabolism-related genes. Results are expressed as fold mRNA expression, where each MYC siRNA condition was normalized to its respective unspecific sequence. Data are presented as mean \pm SD ($n = 3$). * $p < 0.05$, ** $p < 0.01$, *** $p < 0.001$. *ACAA1*, acetyl-CoA acyltransferase 1; *ACAA2*, acetyl-CoA acyltransferase 2; *ACAD9*, acyl-CoA dehydrogenase family, member 9; *ACAD10*, acyl-CoA dehydrogenase family, member 10; *ACAD11*, acyl-CoA dehydrogenase family, member 11; *ACADM*, acyl-CoA dehydrogenase, C-4 to C-12 straight chain; *ACADSB*, acyl-CoA dehydrogenase, short/branched chain; *ACADVL*, acyl-CoA dehydrogenase, very long chain; *ACOD*, cis-aconitate decarboxylase; *ACOX1*, acyl-CoA oxidase 1, palmitoyl; *ACOX2*, acyl-CoA oxidase 2, branched chain; *ACOX3*, acyl-CoA oxidase 3, pristanoyl; *ACSBG1*, acyl-CoA synthetase bubblegum family member 1; *ACSL3*, acyl-CoA synthetase long-chain family member 3; *ACSL5*, acyl-CoA synthetase long-chain family member 5; *BDH2*, 3-hydroxybutyrate dehydrogenase, type 2; *CPT1A*, carnitine palmitoyltransferase 1 A (liver); *CPT1C*, carnitine palmitoyltransferase 1C; *DGLB*, diacylglycerol lipase-beta; *ECHA*, trifunctional enzyme subunit alpha, mitochondrial; *ECI1*, enoyl-CoA delta isomerase 1, mitochondrial; *ECI2*, enoyl-CoA delta isomerase 2; *ETFA*, electron transfer flavoprotein subunit alpha, mitochondrial; *ECH1*, delta(3,5)-delta(2,4)-dienoyl-CoA isomerase, mitochondrial; *ECHM*, enoyl-CoA hydratase, mitochondrial; *FABP1*, fatty acid binding protein 1, liver; *FASN*, fatty acid synthase; *HCD2*, 3-hydroxyacyl-CoA dehydrogenase type-2; *IVD*, isovaleryl-CoA dehydrogenase, mitochondrial; *MCEE*, methylmalonyl CoA epimerase; *MUT*, methylmalonyl CoA mutase; *PECR*, peroxisomal trans-2-enoyl-CoA reductase; *PPARA*, peroxisome proliferator activated receptor alpha; *PPARD*, peroxisome proliferator-activated receptor delta; *PPARG*, peroxisome proliferator activated receptor gamma; *PRKAA1*, protein kinase, AMP-activated, alpha 1 catalytic subunit; *PRKAA2*, protein kinase, AMP-activated, alpha 2 catalytic subunit; *PRKAG1*, protein kinase, AMP-activated, gamma 1 non-catalytic subunit; *SLC27A2*, solute carrier family 27 (fatty acid transporter), member 2.

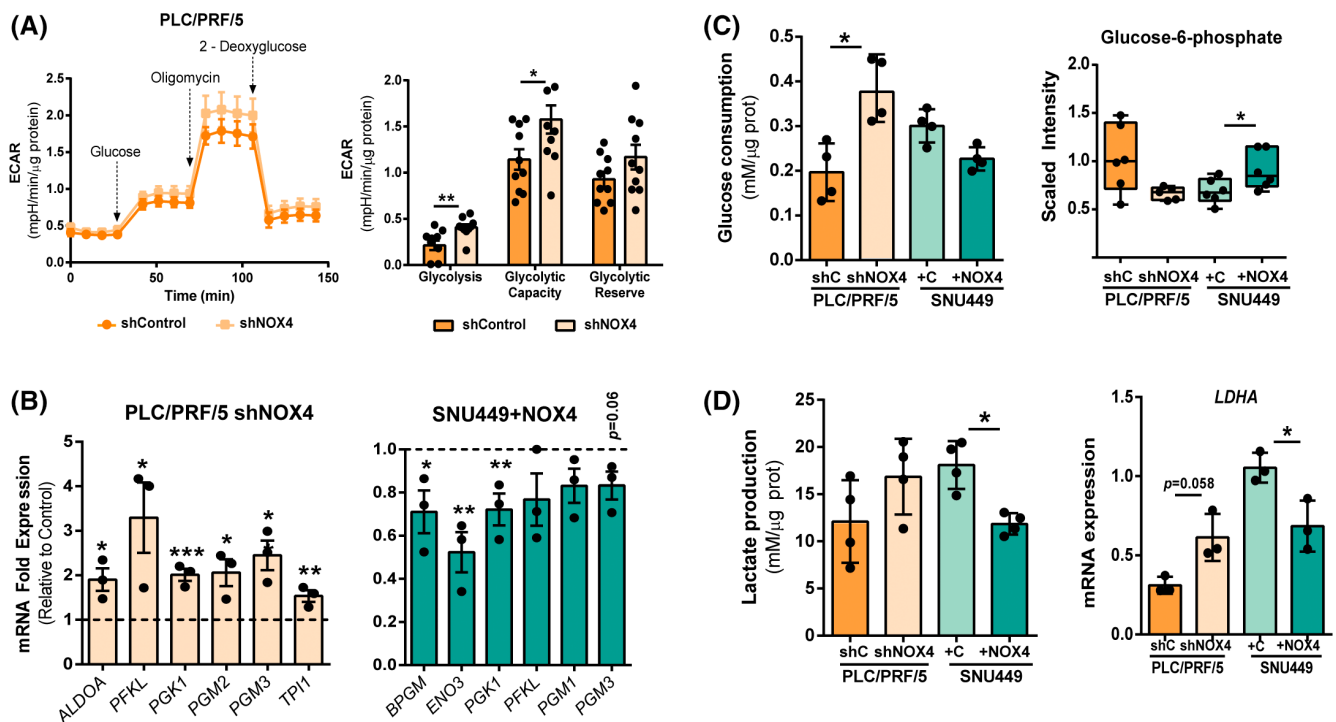


FIGURE 6 NOX4 levels inversely correlate with glycolysis and alters glucose consumption and lactate production in HCC cells. (A) Seahorse analysis of glycolysis in PLC/PRF/5 cells. Left: Continuous extracellular acidification rate (ECAR) values (mpH/min/ μ g protein) are shown. Data are presented as mean \pm SEM ($n = 9-10$). Right: Bar graphs of glycolytic functions were analyzed as explained in the Supporting Information. (B) mRNA fold expression of genes related to glucose metabolism in PLC/PRF/5 shNOX4 (left) and SNU449+NOX4 (right), relative to each respective control. Data are presented as mean \pm SD ($n = 3$). (C) Left: Glucose consumption under basal conditions and normalized to protein content. Data are presented as mean \pm SD ($n = 3$). Right: Glucose-6-phosphate metabolite is depicted by a box plot with whiskers (min to max) ($n = 6$ for each group). (D) Left: Lactate production under basal conditions and normalized to protein content. Data are presented as mean \pm SD ($n = 3$). Right: Relative lactate dehydrogenase A (*LDHA*) mRNA expression. Data are presented as mean \pm SD ($n = 3$). * $p < 0.05$, ** $p < 0.01$, *** $p < 0.001$

PRF/5shNOX4 cells (Figure S14). Additionally, as observed in the proteomic analysis (Figure S11), NOX4 appears to contribute to the function of the proteasome

pathway, which in turn regulates Nrf2 levels. In fact, proteasome activity is decreased in PLC/PRF/5 shNOX4 cells and increased in NOX4-overexpressing SNU449

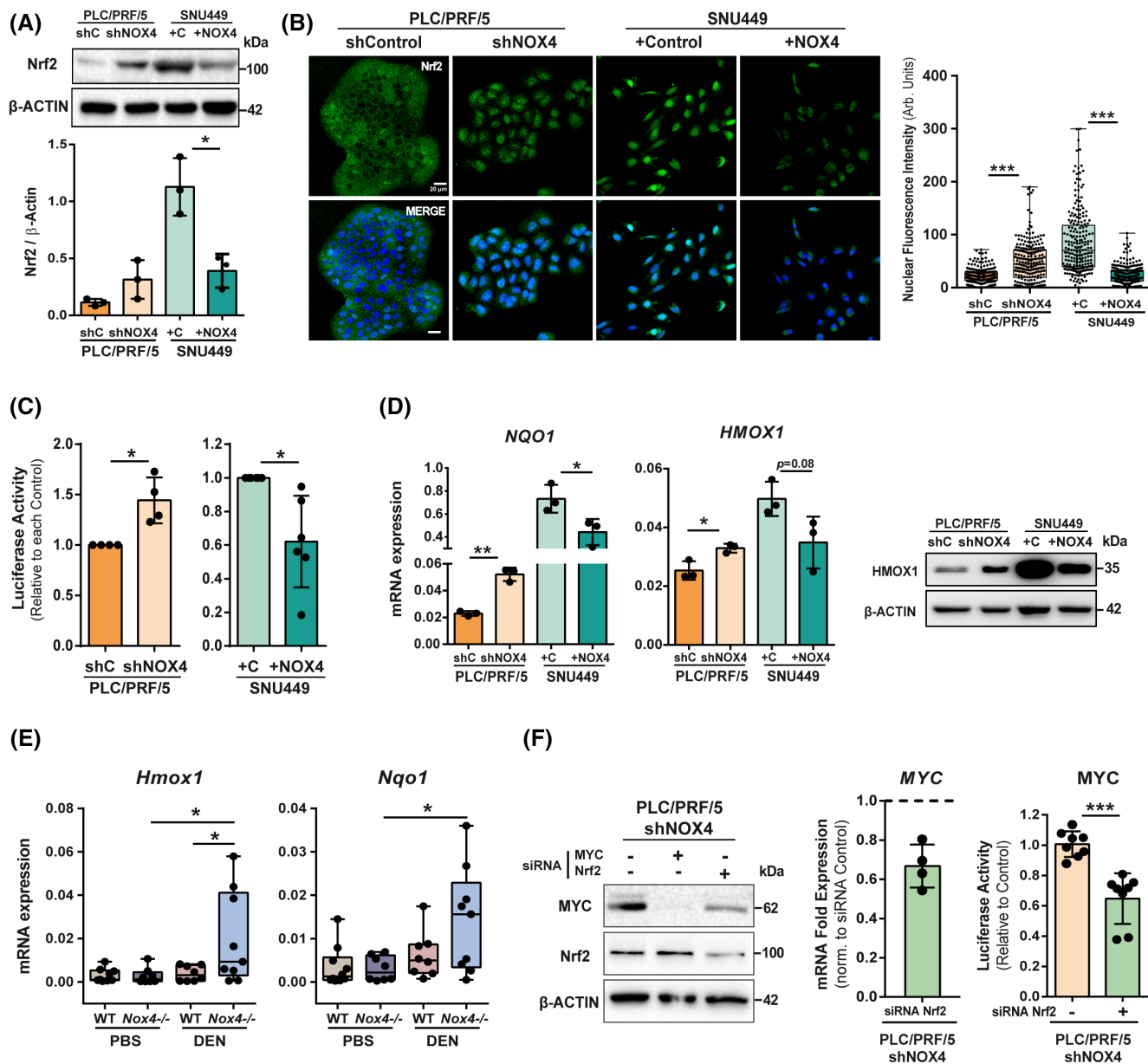
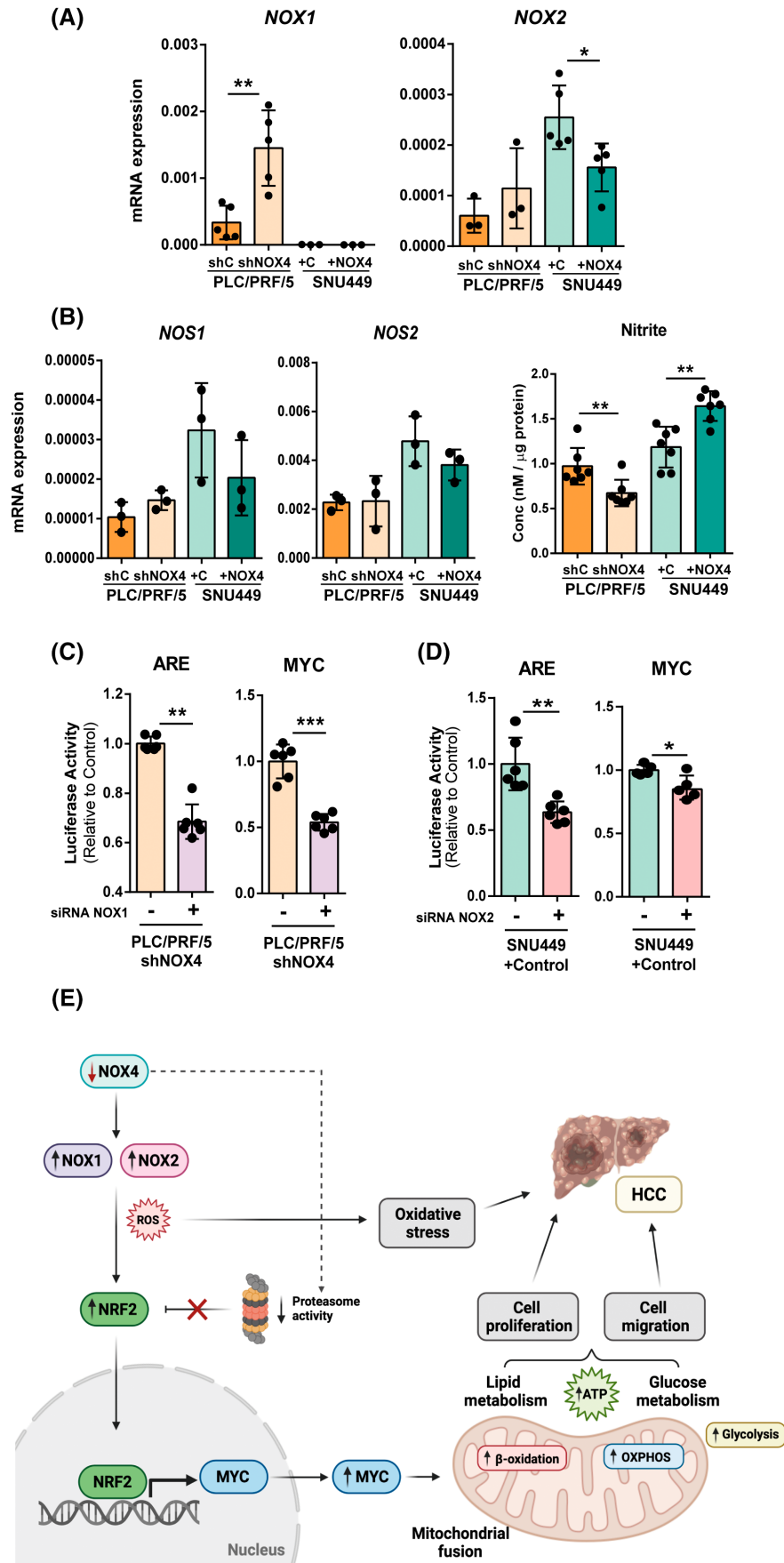


FIGURE 7 Nrf2 expression and activation inversely correlate with NOX4 levels. Cross-talk with the MYC pathway. (A) Top: Nrf2 protein levels. β -Actin was used as loading control. Bottom: Densitometric analysis, expressed as relative to β -actin. Data are presented as mean \pm SD ($n = 3$). (B) Left: Immunofluorescence of Nrf2 (green) and DAPI (blue) for nuclei staining. Scale bar, 20 μ m. Right: Quantification of nuclear fluorescence intensity. Each dot represents one nucleus from independent experiments ($n = 3$). (C) Transcriptional antioxidant response element (ARE) activity. Results are shown relative to each control. Data are presented as mean \pm SD ($n = 4-6$). (D) *NQO1* and *HMOX1* mRNA expression. Data are presented as mean \pm SD ($n = 3$). Right: HMOX1 protein levels. β -Actin was used as loading control. (E) *Hmx1* and *Nqo1* mRNA expression in PBS-treated livers and DEN-induced tumors from WT and *Nox4*^{-/-} mice at 11 months following DEN treatment. Data are presented as relative expression and presented as box plots with whiskers (min to max) ($n = 9$; 3 lysates from 3 different animals). (F) PLC/PRF/5 shNOX4 cells were transiently transfected either with control, MYC, or Nrf2-specific siRNA sequences for 72 h. Left: MYC and Nrf2 protein levels. β -Actin was used as loading control. A representative experiment is shown. Middle: *MYC* mRNA expression expressed as Nrf2 siRNA versus unspecific siRNA. Data are presented as mean \pm SD ($n = 4$). Right: Transcriptional MYC activity. Data are presented as mean \pm SD ($n = 8$). * $p < 0.05$, ** $p < 0.01$, *** $p < 0.001$

FIGURE 8 NOX1 and NOX2 induce Nrf2 and MYC transcriptional activity in HCC cells. (A) *NOX1*, *NOX2*, and nitric oxide synthase 1 (*NOS1*) and nitric oxide synthase 2 (*NOS2*) (left and middle) mRNA expression analyzed by real-time quantitative PCR. Data are presented as mean \pm SD ($n = 3-5$). (B) Right: Extracellular nitrite levels analyzed using the Griess reaction. Data are presented as mean \pm SD ($n = 7$). (C) PLC/PRF/5 shNOX4 (C) and (D) SNU449 + Control (D) cells were transiently transfected either with control or NOX1 (C) or NOX2 specific (D) siRNA sequences for 72 h. Left: Transcriptional ARE activity. Right: Transcriptional MYC activity. Results are shown relative to each control. Data are presented as mean \pm SD ($n = 6$). * $p < 0.05$, ** $p < 0.01$, *** $p < 0.001$. (E) Graphical summary. Image created using BioRender software (<https://www.biorender.com>)



cells (Figure S15). Inhibiting the proteasome with MG132 had a great impact on Nrf2 and MYC levels in the PLC/PRF/5 control cells; however, change in the levels of Nrf2 and MYC was modest in the PLC/PRF/5 shNOX4 cells, correlating with the lower proteasome activity observed in these cells (Figure S15).

Overall, these results point to NOX1/NOX2 as ROS-producing enzymes responsible for oxidative stress and Nrf2 activation in HCC cells with low levels of NOX4. In parallel, NOX4 regulates the proteasome activity, which also affects the Nrf2 levels. Activation of the Nrf2 pathway induces MYC expression and activity, which increases oxidative metabolism, use of lipids and glucose as energy source, and increases ATP levels. All of these changes contribute to the higher capacity of cells to proliferate and migrate (Figure 8E).

DISCUSSION

A specific role for oxidative stress in chronic liver diseases, and as a risk factor for accelerated evolution of HCC, is supported by numerous experimental and clinical studies.^[19] However, ROS are also essential for adequate signal transduction and regulate crucial processes that control tissue homeostasis, such as quiescence, differentiation, senescence, or apoptosis.^[20] NOXs are enzymes producing ROS (superoxide, hydrogen peroxide), whose abundance in liver cells has been frequently associated with inflammation and immune responses. However, the different NOX family members play different roles, are differentially regulated, and localize in different membrane compartments within the liver cell.^[21] In this regard, strong evidence supports differential roles for NOXs in liver cancer, with NOX1 and NOX2 playing detrimental roles, whereas increased NOX4 plays a suppressor role as higher NOX4 expression correlates with better prognosis.^[5–9] NOX4 is an oddity among members of the NOX family, as it is constitutively active. All other NOX enzymes require upstream activators, either calcium, phosphorylations and/or organizer/activator subunits, whereas NOX4 is only associated with the protein p22phox on internal membranes, where ROS generation occurs.^[22,23]

Here we show that loss of NOX4 induces MYC expression and activity, as observed in different HCC cell lines and in a model of experimental hepatocarcinogenesis induced by DEN in *Nox4*-deficient mice. Tumors in these mice show larger size and increased percentage of proliferative cells, when compared with WT mice. Moreover, the analysis of a cohort of patients with HCC indicates an inverse correlation between *NOX4* and *MYC* expression, with patients with low *NOX4* and high *MYC* (T/NT) expression showing a worse relapse-free prognosis, higher probability of microvascular invasion, and advanced tumor grade.

It is well known that MYC plays an essential role during malignant conversion in human hepatocarcinogenesis.^[24] Here we show that MYC, which is required for the increase in migration and invasion observed in NOX4-knockdown HCC cells, is responsible for changes in mitochondrial plasticity, increase in OCR consumption, and transcriptional reprogramming of genes related to oxidative metabolism. Interestingly, the increase in OCR observed in shNOX4 cells occurs simultaneously with the increase in ECAR, reflecting glycolysis activity, and this increase is also impaired after MYC knockdown. It is worthy to note that loss of NOX4 could clearly promote higher catabolism of both glucose and free FA, and, overall, higher ATP production. Different reports in the literature support that MYC frequently induces a hybrid energetics program. Cell reprogramming induces MYC-dependent mitochondrial changes, correlating with up-regulation of both glycolysis and OXPHOS enzymatic machineries.^[25] MYC-overexpressing triple-negative breast cancer shows an increased bioenergetic reliance on FAO, and pharmacological inhibition of MYC catastrophically decreased energy metabolism.^[26] Similar results have been found in MYC-induced lymphomagenesis.^[27] MYC is a major transcriptional target for β -catenin. Interestingly, β -catenin-activated HCC are not glycolytic, but extensively oxidize free FA as fuel for OXPHOS under the control of PPAR α .^[28] Our data would indicate that loss of NOX4 promotes a metabolic reprogramming, reminiscent of the one observed in β -catenin/MYC HCC tumors.^[14]

Data herein point to activation of the Nrf2 pathway concomitant to loss of NOX4, both *in vitro* (NOX4 loss or gain of function models), as well as in two different *in vivo* models (DEN-induced experimental carcinogenesis in *Nox4*-deficient mice and subcutaneous injection of control and NOX4-knockdown Hep3B cells). Furthermore, Nrf2 serves as the connection between NOX4 and MYC. In fact, loss of NOX4 produces an increased oxidative cellular environment, correlating with high Nrf2 protein levels and activity, which is required for the increase in MYC expression and activity. Previous results support a role for NOX4 in regulating Nrf2 and metabolism. Indeed, an increase in mitochondrial oxygen consumption and reserve capacity was observed in murine and human fibroblasts with genetic deficiency or silencing of NOX4,^[29] where the increase in mitochondrial bioenergetics as well as the increase in mitochondrial proteins were inhibited by silencing Nrf2. Our data indicate that NOX4 expression levels (and likely NOX4 activity) counteract the expression of other members of the NOX family, such as NOX1 and NOX2. Silencing NOX1 in HCC cells in which NOX4 had been knocked down prevented Nrf2 activation and MYC up-regulation. NOX4 and NOX1 play opposite roles in HCC cells. NOX4 mediates the pro-apoptotic and pro-senescence effects of the TGF- β ,^[30,31] and its

depletion induces higher proliferation and invasion.^[8,9] On the contrary, NOX1 mediates autocrine growth and survival of liver tumor cells and anti-apoptotic signals induced by TGF- β through the transactivation of the EGF receptor pathway.^[32,33] Indeed, NOX1 pharmacological inhibition impairs cell growth and enhances TGF- β -induced apoptosis,^[34] and attenuates the development of a pro-tumorigenic environment in experimental HCC.^[35] Overall, NOX1 and NOX4 exert opposite roles in the control of liver growth and apoptosis, and their balance may dictate cell fate. Furthermore, it is worthy to note that NOX4 activity may be regulated by cellular pO₂, allowing it to function as an O₂ sensor. NOX4 has an unusually high K_M for O₂ (~18%), which may allow NOX4 to generate H₂O₂ as a function of O₂ concentration throughout a physiological range of pO₂ values and to respond rapidly to changes in pO₂.^[23] Indeed, loss of NOX4 may induce the expression of other NOX enzymes and, simultaneously, could deprive the cell of the O₂ sensor system that could provoke an oxygen-rich, pro-oxidative intracellular environment. Supporting this idea, a protective role of NOX4 by reducing oxidative DNA damage and the risk of carcinogen-induced tumor formation was reported.^[36]

Our studies indicate that NOX4 deficiency in patients with HCC may generate dysregulation of the redox balance and activation of the Nrf2 and MYC pathways, which regulate mitochondrial dynamics, oxygen consumption, and a metabolic shift to enhanced glucose and FA use and higher ATP production. New therapeutic prospects may open up for this cohort of HCC patients with low expression of NOX4, as it could be treatable with drugs targeting mitochondrial metabolism,^[37] such as metformin or CPI-613, a lipoate analog that inhibits mitochondrial enzymes, or the recently advanced β -adrenergic blocker neivolol that simultaneously targets OXPHOS and angiogenesis to arrest tumor growth.^[38] In parallel, the described inverse regulation between NOX4 and other members of the NOX family provides a rationale for the use of NOX1/NOX2 inhibitors^[39] as therapeutic drugs in this specific cohort of patients with low-NOX4 HCC, or for the use of NOX1/NOX4 inhibitors for liver fibrosis, which would prevent not only myofibroblast activation but also the appearance of NOX1-dependent neoplastic transformation.

AUTHOR CONTRIBUTIONS

Study design, funding obtainment, and study supervision: Isabel Fabregat. *Experiments:* Irene Peñuelas-Haro and Esther Bertran. *Cell line obtainment and initial proteomic and metabolomic analyses:* Eva Crosas-Molist. *In vivo experiments in Nox4^{-/-} mice:* Rut Espinosa-Sotelo, Macarena Herranz-Itúrbide, and Daniel Caballero-Díaz. *Analyses in human tissues from patients with HCC:* Emilio Ramos and Teresa Serrano. Mitochondrial and Seahorse metabolic analyses were performed in the JMC Lab and AZ Lab, respectively.

The analysis of redox metabolism was performed in the UGK lab. *Data interpretation:* María L. Martínez-Chantar, José M. Cuezva, Antonio Zorzano, and Ulla G. Knaus. *Bioinformatic analysis:* Ania Alay and Xavier Solé. *Manuscript draft:* Irene Peñuelas-Haro and Isabel Fabregat. *Critical revisions for important intellectual content:* Esther Bertran, José M. Cuezva, Antonio Zorzano, and Ulla G. Knaus. The final manuscript was approved by all of the authors.

ACKNOWLEDGMENT

The authors thank Dr. Jitka Soukupova for advising and teaching in the initial metabolism experiments and Dr. Àngels Fabra for advising in the *in vivo* xenografts experiments. They also acknowledge the Scientific and Technical Services of IDIBELL, in particular the Animal Facility, Microscopy, and Molecular Interactions Services, as well as the Scientific and Technological Centers of the University of Barcelona for confocal microscopy support.

FUNDING INFORMATION

Supported by Agencia Estatal de Investigación, Ministerio de Ciencia e Innovación, Spain (co-funded by European Regional Development Fund ERDF, a way to build Europe) (SAF2015-64149-R, RTI2018-094079-B-100, PID2021-122551OB-I00, PID2019-106209RB-I00, PID2019-108674RB-100, and RED2018-102576-T); FPI fellowships (BES-2016-077564 and PRE2019-089144); the Generalitat de Catalunya (2017SGR1015); Science Foundation Ireland (16/IA/4501); CIBER, National Biomedical Research Institute, which is funded by the Instituto de Salud Carlos III, Spain; CERCA Programme/Generalitat de Catalunya; and an ICREA "Academia" Award (Generalitat de Catalunya).

CONFLICT OF INTEREST

Nothing to report.

ORCID

María L. Martínez-Chantar  <https://orcid.org/0000-0002-6446-9911>

[org/0000-0002-6446-9911](https://orcid.org/0000-0002-6446-9911)

Isabel Fabregat  <https://orcid.org/0000-0003-0136-8440>

[org/0000-0003-0136-8440](https://orcid.org/0000-0003-0136-8440)

REFERENCES

1. Müller M, Bird TG, Nault JC. The landscape of gene mutations in cirrhosis and hepatocellular carcinoma. *J Hepatol.* 2020;72:990–1002.
2. Leone V, Ali A, Weber A, Tschaharganeh DF, Heikenwalder M. Liver Inflammation and Hepatobiliary Cancers. *Trends Cancer.* 2021;7:606–23.
3. Schröder K. NADPH oxidases: current aspects and tools. *Redox Biol.* 2020;34:101512.
4. Buvelot H, Jaquet V, Krause KH. Mammalian NADPH oxidases. In: Knaus UG, Leto TL, editors. *NADPH Oxidases*. Vol 1982. *Methods in Molecular Biology*. New York: Springer; 2019. p. 17–36.

5. Gabbia D, Cannella L, De Martin S. The role of oxidative stress in NAFLD–NASH–HCC transition—focus on NADPH oxidases. *Biomedicine*. 2021;9:687.
6. Ha SY, Paik YH, Yang JW, Lee MJ, Bae H, Park CK. NADPH oxidase 1 and NADPH oxidase 4 have opposite prognostic effects for patients with hepatocellular carcinoma after hepatectomy. *Gut Liver*. 2016;10:826–35.
7. Eun HS, Cho SY, Joo JS, Kang SH, Moon HS, Lee ES, et al. Gene expression of NOX family members and their clinical significance in hepatocellular carcinoma. *Sci Rep*. 2017;7:11060.
8. Crosas-Molist E, Bertran E, Rodriguez-Hernandez I, Herraiz C, Cantelli G, Fabra A, et al. The NADPH oxidase NOX4 represses epithelial to amoeboid transition and efficient tumour dissemination. *Oncogene*. 2017;36:3002–14.
9. Crosas-Molist E, Bertran E, Sancho P, López-Luque J, Fernando J, Sánchez A, et al. The NADPH oxidase NOX4 inhibits hepatocyte proliferation and liver cancer progression. *Free Radic Biol Med*. 2014;69:338–47.
10. Herranz-Iturbide M, López-Luque J, Gonzalez-Sanchez E, Caballero-Díaz C, Crosas-Molist E, Martín-Mur B, et al. NADPH oxidase 4 (Nox4) deletion accelerates liver regeneration in mice. *Redox Biol*. 2021;40:101841.
11. de Matteis S, Ragusa A, Marisi G, de Domenico S, Casadei Gardini A, Bonafè M, et al. Aberrant metabolism in hepatocellular carcinoma provides diagnostic and therapeutic opportunities. Egea J, ed. *Oxid Med Cell Longev*. 2018;2018:7512159.
12. Tenen DG, Chai L, Tan JL. Metabolic alterations and vulnerabilities in hepatocellular carcinoma. *Gastroenterol Rep*. 2021;9:1–13.
13. Beyoğlu D, Imbeaud S, Maurhofer O, Bioulac-Sage P, Zucman-Rossi J, Dufour JF, et al. Tissue metabolomics of hepatocellular carcinoma: tumor energy metabolism and the role of transcriptomic classification. *Hepatology*. 2013;58:229–38.
14. Nakagawa H, Hayata Y, Kawamura S, Yamada T, Fujiwara N, Koike K. Lipid metabolic reprogramming in hepatocellular carcinoma. *Cancer*. 2018;10:447.
15. Soukupova J, Malfettone A, Hyroššová P, Hernández-Alvarez MI, Peñuelas-Haro I, Bertran E, et al. Role of the transforming growth factor- β in regulating hepatocellular carcinoma oxidative metabolism. *Sci Rep*. 2017;7:12486.
16. Sancho P, Bertran E, Caja L, Carmona-Cuenca I, Murillo MM, Fabregat I. The inhibition of the epidermal growth factor (EGF) pathway enhances TGF- β -induced apoptosis in rat hepatoma cells through inducing oxidative stress coincident with a change in the expression pattern of the NADPH oxidases (NOX) isoforms. *Biochim Biophys Acta BBA - Mol Cell Res*. 2009;1793:253–63.
17. Sancho P, Martín-Sanz P, Fabregat I. Reciprocal regulation of NADPH oxidases and the cyclooxygenase-2 pathway. *Free Radic Biol Med*. 2011;51:1789–98.
18. Caja L, Sancho P, Bertran E, Iglesias-Serret D, Gil J, Fabregat I. Overactivation of the MEK/ERK pathway in liver tumor cells confers resistance to TGF- β -induced cell death through impairing up-regulation of the NADPH oxidase NOX4. *Cancer Res*. 2009;69:7595–602.
19. Borrelli A, Bonelli P, Tuccillo FM, Goldfine ID, Evans JL, Buonaguro FM, et al. Role of gut microbiota and oxidative stress in the progression of non-alcoholic fatty liver disease to hepatocarcinoma: current and innovative therapeutic approaches. *Redox Biol*. 2018;15:467–79.
20. Helfinger V, Schröder K. Redox control in cancer development and progression. *Mol Aspects Med*. 2018;63:88–98.
21. Herranz-Iturbide M, Peñuelas-Haro I, Espinosa-Sotelo R, Bertran E, Fabregat I. The TGF- β /NADPH oxidases axis in the regulation of liver cell biology in health and disease. *Cell*. 2021;10:2312.
22. Martyn KD, Frederick LM, von Loehneysen K, Dinauer MC, Knaus UG. Functional analysis of Nox4 reveals unique characteristics compared to other NADPH oxidases. *Cell Signal*. 2006;18:69–82.
23. Nisimoto Y, Diebold BA, Cosentino-Gomes D, Lambeth JD. Nox4: a hydrogen peroxide-generating oxygen sensor. *Biochemistry*. 2014;53:5111–20.
24. Kaposi-Novak P, Libbrecht L, Woo HG, Lee YH, Sears NC, Coulouarn C, et al. Central role of c-Myc during malignant conversion in human hepatocarcinogenesis. *Cancer Res*. 2009;69:2775–82.
25. Prieto J, Seo AY, León M, Santacatterina F, Torresano L, Palomino-Schätzlein M, et al. MYC induces a hybrid energetics program early in cell reprogramming. *Stem Cell Rep*. 2018;11:1479–92.
26. Camarda R, Zhou AY, Kohnz RA, Balakrishnan S, Mahieu C, Anderton B, et al. Inhibition of fatty acid oxidation as a therapy for MYC-overexpressing triple-negative breast cancer. *Nat Med*. 2016;22:427–32.
27. Pacilli A, Calienni M, Margarucci S, D'Apolito M, Petillo O, Rocchi L, et al. Carnitine-acyltransferase system inhibition, cancer cell death, and prevention of myc-induced lymphomagenesis. *JNCI J Natl Cancer Inst*. 2013;105:489–98.
28. Senni N, Savall M, Cabrerizo Granados D, Alves-Guerra MC, Sartor C, Lagoutte I, et al. β -catenin-activated hepatocellular carcinomas are addicted to fatty acids. *Gut*. 2019;68:322–34.
29. Bernard K, Logsdon NJ, Miguel V, Benavides GA, Zhang J, Carter AB, et al. NADPH oxidase 4 (Nox4) suppresses mitochondrial biogenesis and bioenergetics in lung fibroblasts via a nuclear factor erythroid-derived 2-like 2 (Nrf2)-dependent pathway. *J Biol Chem*. 2017;292:3029–38.
30. Carmona-Cuenca I, Roncero C, Sancho P, Caja L, Fausto N, Fernández M, et al. Upregulation of the NADPH oxidase NOX4 by TGF- β in hepatocytes is required for its pro-apoptotic activity. *J Hepatol*. 2008;49:965–76.
31. Senturk S, Mumcuoglu M, Gursoy-Yuzugullu O, Cingoz B, Akcali KC, Ozturk M. Transforming growth factor-beta induces senescence in hepatocellular carcinoma cells and inhibits tumor growth. *Hepatology*. 2010;52:966–74.
32. Sancho P, Fabregat I. NADPH oxidase NOX1 controls autocrine growth of liver tumor cells through up-regulation of the epidermal growth factor receptor pathway. *J Biol Chem*. 2010;285:24815–24.
33. Moreno-Cáceres J, Mainez J, Mayoral R, Martín-Sanz P, Egea G, Fabregat I. Caveolin-1-dependent activation of the metalloprotease TACE/ADAM17 by TGF- β in hepatocytes requires activation of Src and the NADPH oxidase NOX1. *FEBS J*. 2016;283:1300–10.
34. Sancho P, Fabregat I. The NADPH oxidase inhibitor VAS2870 impairs cell growth and enhances TGF- β -induced apoptosis of liver tumor cells. *Biochem Pharmacol*. 2011;81:917–24.
35. Vandierendonck A, Degroote H, Vanderborcht B, Verhelst X, Geerts A, Devisscher L, et al. NOX1 inhibition attenuates the development of a pro-tumorigenic environment in experimental hepatocellular carcinoma. *J Exp Clin Cancer Res*. 2021;40:40.
36. Helfinger V, Freiherr von Gall F, Henke N, Kunze MM, Schmid T, Rezende F, et al. Genetic deletion of Nox4 enhances cancerogen-induced formation of solid tumors. *Proc Natl Acad Sci*. 2021;118:e2020152118.
37. Vasan K, Werner M, Chandel NS. Mitochondrial metabolism as a target for cancer therapy. *Cell Metab*. 2020;32:341–52.
38. Nuevo-Tapióles C, Santacatterina F, Stamatakis K, Núñez de Arenas C, Gómez de Cedrón M, Formentini L, et al. Coordinate β -adrenergic inhibition of mitochondrial activity and angiogenesis arrest tumor growth. *Nat Commun*. 2020;11:3606.
39. Elbatreek MH, Mucke H, Schmidt HHHW. NOX inhibitors: from bench to naxibs to bedside. In: Schmidt HHHW,

Ghezzi P, Cuadrado A, eds. Reactive Oxygen Species. Vol 264. Handbook of Experimental Pharmacology. Heidelberg: Springer International Publishing; 2020:145–68.

SUPPORTING INFORMATION

Additional supporting information can be found online in the Supporting Information section at the end of this article.

How to cite this article: Peñuelas-Haro I, Espinosa-Sotelo R, Crosas-Molist E, Herranz-Iturbide M, Caballero-Díaz D & Alay A et al. The NADPH oxidase NOX4 regulates redox and metabolic homeostasis preventing HCC progression. *Hepatology*. 2022;00:1–19. <https://doi.org/10.1002/hep.32702>